# An Outward-Wave-Favouring Finite Element-Based Strategy for Exterior Acoustical Problems

**C. S. Jog**

*Facility for Research in Technical Acoustics (FRITA), Dept. of Mechanical Engg., Indian Institute of Science, Bangalore 560012, India*

(Received 30 November 2011, revised 10 September 2012, accepted 14 November 2012)

This work presents a finite element-based strategy for exterior acoustical problems based on an assumed pressure form that favours outgoing waves. The resulting governing equation, weak formulation, and finite element formulation are developed both for coupled and uncoupled problems. The developed elements are very similar to conventional elements in that they are based on the standard Galerkin variational formulation and use standard Lagrange interpolation functions and standard Gaussian quadrature. In addition and in contrast to wave envelope formulations and their extensions, the developed elements can be used in the immediate vicinity of the radiator/scatterer. The method is similar to the perfectly matched layer (PML) method in the sense that each layer of elements added around the radiator absorbs acoustical waves so that no boundary condition needs to be applied at the outermost boundary where the domain is truncated. By comparing against strategies such as the PML and wave-envelope methods, we show that the relative accuracy, both in the near and far-field results, is considerably higher.

## 1. INTRODUCTION

The main difficulty that arises in solving exterior acoustical problems is the unboundedness of the domain. Although the boundary element method yields accurate results, the computational cost and memory requirements for large-scale problems can be prohibitive. Finite element methods can be more cost-effective due to the sparse nature of the matrices. Among the finite element-based techniques, one popular approach has been to truncate the computational domain at some distance away from the radiator or scatterer, and to impose a boundary condition at this artificial boundary (see Givoli[1] for a description of the classical approaches and to Qi and Geers[2] for a relatively recent approach known as the perfectly matched layer (PML)). Yet another approach involves infinite elements.[3–9] Both approaches have their merits and demerits, which have been discussed in detail in the references cited.

Most of the work towards improving the former approach has focused either on devising and implementing higher-order absorbing conditions or on modifying these conditions to make them applicable for non-spherical truncation boundaries. The goal in this study is to improve upon the former approach, not by modifying the boundary conditions, but by modifying the function that is being solved for, namely the pressure field. The assumed form of the pressure field favours outgoing waves, which makes it easier for the resulting finite element formulation to capture the solution. Summarizing, note the following:

1. The proposed formulation is a modification of the conventional approach based on absorbing boundary conditions; the computational domain and input data are exactly the same; and the computational cost is also almost the same as for the conventional formulation.

2. The most crucial aspect of the proposed formulation is that it is based on a Cartesian framework and, thus, avoids the cumbersome use of angular coordinates and the problems associated with them. In particular, it allows the elements to be used directly in the vicinity of the radiator or scatterer, which is in contrast to existing wave envelope and related formulations, where an inner mesh of conventional elements has to be used, leading to poorer accuracy (see section 4.2 for a comparison). In addition, there is no problem of ill-conditioning, as for example, occurs in the radial-direction matrices in some infinite finite element formulations (see, e.g., Bhandakkar and Jog[9] and Dreyer and Estorff[10]). Although researches have attempted to alleviate this ill-conditioning[10] the fact remains that non-standard interpolations, such as Legendre or Jacobi polynomials, must be used.

3. Since an oscillatory part is separated out in the proposed formulation, the resulting finite element formulation has to capture a more gently varying function in most problems, resulting in much higher accuracy compared to the conventional formulation. In this connection, I mention that both the near- and far-field results presented in this study were obtained from raw nodal values without the use of the Helmholtz integral equation (which can be computationally very expensive to evaluate and which is used to obtain accurate far-field results[3–5]).

4. Since it uses only a first-order (spherical) damper, the implementation is very simple. Similar to the PML method, each layer of elements added around the radiator/scatterer absorbs acoustical waves so that no boundary condition needs to be applied at the truncated boundary. Note that the PML method is not only more complicated but also fails to yield good accuracy even on relatively simple problems, such as the dilatational motion of a spherical surface unless

a large acoustical domain is used.[2] In addition, implementing the PML requires setting several numerical parameters such as the width of the layer and the number of divisions as well as the PML coefficients and their maximal values, requiring an optimization of these parameters.[11,12] Methods that are coupled to the PML inherit its problems. For example, Huttunen, Kaipio, and Monk[13] mention that several PML parameters must be properly adjusted to reduce numerical reflections to an acceptable level. Even after such an optimization is carried out, the accuracy could be poor, even on simple problems, as discussed in section 4.1. In contrast, in the proposed method—apart from the radius of the circumscribing spherical boundary—no factors need to be adjusted by the user.

Section 2 briefly presents the conventional formulation and then the proposed formulation, and section 3 extends the proposed formulation to coupled problems. Section 4 presents several numerical examples involving uncoupled/coupled and radiation/scattering problems. The conclusions are presented in section 5.

## 2. FORMULATION

Before presenting the proposed formulation, I briefly review the conventional formulation involving absorbing boundary conditions on the surface where the infinite domain is truncated. In this work, we consider only the case where the loading, and hence the pressure response, is time-harmonic, i.e.,

$$p = \tilde{p}e^{i\omega t}; \tag{1}$$

where $\omega$ is the angular frequency. The wave equation in this case reduces to the Helmholtz equation given by

$$\boldsymbol{\nabla}^2\tilde{p} + k^2\tilde{p} = 0; \tag{2}$$

where, with $c$ denoting the acoustic wave speed, $k = \omega/c$ is the wave number. Although in interior acoustical problems (in the absence of absorbers), $\tilde{p}$ is real-valued; in the case of the exterior problem being solved in this study, $\tilde{p}$ is complex-valued because of the damping-like effect that arises due to the infinite domain (see Eq. (9) below). If $\Omega$ denotes the domain over which the problem is being solved, $\Gamma$ denotes its boundary and $\boldsymbol{n}$ denotes the unit normal to the boundary, then the variational formulation of the above equation, obtained by multiplying Eq. (2) by the variation $p_\delta$ and carrying out an appropriate integration by parts, is given by

$$\int_\Omega (\boldsymbol{\nabla}p_\delta \cdot \boldsymbol{\nabla}\tilde{p} - k^2 p_\delta \tilde{p})\, d\Omega = \int_\Gamma p_\delta \boldsymbol{\nabla}\tilde{p}\cdot\boldsymbol{n}\, d\Gamma. \tag{3}$$

In an exterior radiation problem, the normal velocity $v_n$ is specified over part of the boundary $\Gamma_r$, while over the part of the boundary $\Gamma_\infty$ where the domain is truncated, appropriate absorbing conditions (see below) that approximate the Sommerfeld radiation condition are specified. In a scattering problem, the total pressure $\tilde{p}$ is assumed to be decomposed into an incident pressure field $p_{\text{inc}}$ and a scattered field $p_{\text{scat}}$, both of which individually satisfy Eq. (2), and the scattered field satisfies the Sommerfeld radiation condition as well. Thus, in the scattering problem, we can solve for the scattered field by replacing $\tilde{p}$ with $p_{\text{scat}}$ in Eq. (3). If the boundary over which the scattering occurs is denoted by $\Gamma_s$ and $u_n$ denotes the normal displacement of the scatterer boundary, then

$$\boldsymbol{\nabla}\tilde{p}\cdot\boldsymbol{n} = \boldsymbol{\nabla}p_{\text{inc}}\cdot\boldsymbol{n} + \boldsymbol{\nabla}p_{\text{scat}}\cdot\boldsymbol{n} = \rho_f\omega^2 u_n;$$

which implies that

$$\boldsymbol{\nabla}p_{\text{scat}}\cdot\boldsymbol{n} = -\boldsymbol{\nabla}p_{\text{inc}}\cdot\boldsymbol{n} + \rho_f\omega^2 u_n.$$

Thus, with $\rho_f$ denoting the density of the acoustical fluid, the boundary conditions on the radiating and scattering surfaces $\Gamma_r$ and $\Gamma_s$ are

$$\boldsymbol{\nabla}\tilde{p}\cdot\boldsymbol{n} = -\rho_f i\omega v_n \qquad \text{(radiation);} \tag{4a}$$

$$\boldsymbol{\nabla}p_{\text{scat}}\cdot\boldsymbol{n} = -\boldsymbol{\nabla}p_{\text{inc}}\cdot\boldsymbol{n} + \rho_f\omega^2 u_n \qquad \text{(scatterer).} \tag{4b}$$

If, for example, the incident wave is a plane wave of the form

$$p_{\text{inc}} = p_i e^{i\boldsymbol{k}\cdot\boldsymbol{x}}; \tag{5}$$

where $\boldsymbol{x}$ is the position vector, then

$$\boldsymbol{\nabla}p_{\text{inc}}\cdot\boldsymbol{n} = p_i i(\boldsymbol{k}\cdot\boldsymbol{n})e^{i\boldsymbol{k}\cdot\boldsymbol{x}}.$$

Although I present the formulation for the radiation problem below, the formulation for the scattering problem can be obtained by replacing $\tilde{p}$ with $p_{\text{scat}}$. I take $\Gamma_\infty$ to be a sphere of radius $R$ throughout this work and use a spherical damper of the form used by Bayliss and Turkel[14]:

$$\boldsymbol{\nabla}\tilde{p}\cdot\boldsymbol{n} = -\frac{\tilde{p}}{R} - ik\tilde{p}. \tag{6}$$

The finite element formulation is obtained by discretizing the pressure field and its variation as

$$\tilde{p} = \boldsymbol{N}_p\hat{\boldsymbol{p}}, \qquad p_\delta = \boldsymbol{N}_p\hat{\boldsymbol{p}}_\delta; \tag{7a}$$

$$\boldsymbol{\nabla}\tilde{p} = \boldsymbol{B}_p\hat{\boldsymbol{p}}, \qquad \boldsymbol{\nabla}p_\delta = \boldsymbol{B}_p\hat{\boldsymbol{p}}_\delta; \tag{7b}$$

where $\boldsymbol{N}_p = [N_1 \quad N_2 \quad \dots\ ]$ is the standard Lagrange shape function matrix, and

$$\boldsymbol{B}_p = \begin{bmatrix} \frac{\partial N_1}{\partial x} & \frac{\partial N_2}{\partial x} & \dots \\ \frac{\partial N_1}{\partial y} & \frac{\partial N_2}{\partial y} & \dots \\ \frac{\partial N_1}{\partial z} & \frac{\partial N_2}{\partial z} & \dots \end{bmatrix}. \tag{8}$$

By substituting the above discretizations into Eq. (3) and using the arbitrariness of $\hat{\boldsymbol{p}}_\delta$, we obtain the finite element equations

$$\left[\boldsymbol{K}_p - \omega^2\boldsymbol{M}_p + i\omega\boldsymbol{C}_p\right]\hat{\boldsymbol{p}} = \hat{\boldsymbol{f}}_p; \tag{9}$$

where with $R$ written as $|\boldsymbol{x}|$,

$$\boldsymbol{K}_p = \int_\Omega \boldsymbol{B}_p^T\boldsymbol{B}_p\, d\Omega + \int_{\Gamma_\infty}\frac{1}{|\boldsymbol{x}|}\boldsymbol{N}_p^T\boldsymbol{N}_p\, d\Gamma; \tag{10}$$

$$\boldsymbol{M}_p = \int_\Omega \frac{1}{c^2}\boldsymbol{N}_p^T\boldsymbol{N}_p\, d\Omega; \tag{11}$$

$$\boldsymbol{C}_p = \int_{\Gamma_\infty}\frac{1}{c}\boldsymbol{N}_p^T\boldsymbol{N}_p\, d\Gamma; \tag{12}$$

$$\hat{\boldsymbol{f}}_p = -\int_{\Gamma_r} \rho_f i\omega v_n \boldsymbol{N}_p^T \, d\Gamma. \tag{13}$$

For the scattering problem, where, for example, the incident wave is given by Eq. (5),

$$\hat{\boldsymbol{f}}_p = -\int_{\Gamma_s} p_i i(\boldsymbol{k}\cdot\boldsymbol{n}) e^{i\boldsymbol{k}\cdot\boldsymbol{x}} \boldsymbol{N}_p^T \, d\Gamma.$$

Note that in the above formulation, the damping matrix $\boldsymbol{C}_p$ is exclusively due to the boundary condition on $\Gamma_\infty$. If $(\xi, \eta)$ are the natural coordinates used for parametrizing the surface, then the expressions for the normal and the area element are

$$\boldsymbol{n} = \frac{\frac{\partial \boldsymbol{x}}{\partial \xi} \times \frac{\partial \boldsymbol{x}}{\partial \eta}}{\left\| \frac{\partial \boldsymbol{x}}{\partial \xi} \times \frac{\partial \boldsymbol{x}}{\partial \eta} \right\|};$$

$$d\Gamma = \left\| \frac{\partial \boldsymbol{x}}{\partial \xi} \times \frac{\partial \boldsymbol{x}}{\partial \eta} \right\| d\xi \, d\eta.$$

Since the same interpolation functions are used for $\tilde{p}$ and $p_\delta$ (see Eq. (7a)), the above formulation corresponds to the Bubnov-Galerkin method. Other choices, such as, for example, the interpolation functions for $p_\delta$ and $\tilde{p}$ being complex-conjugates of each other, are also possible; see Astley[15] and Eq. (29).

The proposed formulation is as follows. Instead of the pressure assumed to be of the form given by Eq. (1), we assume it to be of the form

$$p = \frac{1}{|\boldsymbol{x}|} G(\boldsymbol{x}) e^{i(\omega t - k|\boldsymbol{x}|)}; \tag{14}$$

where $|\boldsymbol{x}| = \sqrt{\boldsymbol{x}\cdot\boldsymbol{x}}$, and $G(\boldsymbol{x})$ is an unknown complex-valued function which is to be determined by an approximation strategy such as the finite element method. The above form assumes that the "centre" of the radiating body is at the origin; if instead the centre is at $\boldsymbol{x}_0$, $\boldsymbol{x}$ should be replaced with $\boldsymbol{x} - \boldsymbol{x}_0$ in the above expression. Note the following:

1. The form of the pressure in Eq. (14) favours outgoing waves, while the form in Eq. (1), allows for both incoming and outgoing waves. The spherical damping condition given by Eq. (6) and (15) below leads to the condition $(\boldsymbol{\nabla} G)\cdot\boldsymbol{n} = 0$ on $\Gamma_\infty$. Thus, similar to the PML, no boundary condition needs to be imposed on $\Gamma_\infty$. A higher-order damper was also tried but did not result in any significant improvement in the results.

2. From Atkinson,[16] we know that the far-field pressure is proportional to $e^{-ik|\boldsymbol{x}|}/|\boldsymbol{x}|$, which provides a justification for the use of Eq. (14). In the near-field, of course, the field is generally more complicated, but the function $G(\boldsymbol{x})$ (to be determined) compensates for the difference. The fact that it does so effectively will be shown in section 4 by means of various nontrivial problems in which $G(\boldsymbol{x})$ has a complicated variation.

3. Since the oscillatory part is separated, $G(\boldsymbol{x})$ is a more gently varying function compared to $\tilde{p}$, resulting in higher overall accuracy, as will be clear in section 4.

4. The differences of the proposed formulation from the wave envelope formulation of Astley[17] and Astley and Eversman[18] are discussed at the end of this section.

5. The use of $|\boldsymbol{x}|$ instead of the radial spherical coordinate $r$ is the most critical aspect of the proposed formulation; it ensures that the formulation can be carried out with respect to a Cartesian basis, thus avoiding the use of angular coordinates, which can be quite cumbersome.[9] Since the formulation is then exactly analogous to that for conventional elements, one can use these elements in the direct vicinity of the radiator or scatterer (except when the origin is part of the acoustic domain, in which case, conventional elements are used in the vicinity of the origin as discussed towards the end of this section). Since in most situations, conventional elements do not need to be used at all, the use of the proposed method results in a dramatic reduction in computational cost. In contrast, with most infinite element formulations, one needs a mesh of conventional elements between the radiator/scatterer and a circumscribing boundary such as an ellipsoid, with infinite elements used in the exterior of this boundary. Although there have been attempts to alleviate this problem,[19–21] they involve very complicated formulations.

We now derive the governing equations and boundary conditions for $G(\boldsymbol{x})$. From Eq. (1) and (14), we see that

$$\tilde{p} = \frac{1}{|\boldsymbol{x}|} G(\boldsymbol{x}) e^{-ik|\boldsymbol{x}|}. \tag{15}$$

Using the fact that

$$\boldsymbol{\nabla} |\boldsymbol{x}| = \boldsymbol{x}/|\boldsymbol{x}|$$

and

$$\boldsymbol{\nabla}(1/|\boldsymbol{x}|) = -\boldsymbol{x}/|\boldsymbol{x}|^3;$$

we get

$$\boldsymbol{\nabla}\tilde{p} = \left[\boldsymbol{\nabla} G - \frac{1}{|\boldsymbol{x}|} ik\boldsymbol{x} G - \frac{1}{|\boldsymbol{x}|^2}\boldsymbol{x} G\right] \frac{e^{-ik|\boldsymbol{x}|}}{|\boldsymbol{x}|}; \tag{16}$$

$$\boldsymbol{\nabla}^2\tilde{p} = \left[\boldsymbol{\nabla}^2 G - \frac{2}{|\boldsymbol{x}|} ik\boldsymbol{\nabla} G\cdot\boldsymbol{x} - \frac{2}{|\boldsymbol{x}|^2}\boldsymbol{\nabla} G\cdot\boldsymbol{x} - k^2 G\right] \frac{e^{-ik|\boldsymbol{x}|}}{|\boldsymbol{x}|}. \tag{17}$$

Substituting Eqs. (15) and (17) into Eq. (2), we get the governing equation for $G(\boldsymbol{x})$ as

$$\boldsymbol{\nabla}^2 G - \frac{2}{|\boldsymbol{x}|}\left(ik + \frac{1}{|\boldsymbol{x}|}\right)\boldsymbol{\nabla} G\cdot\boldsymbol{x} = 0. \tag{18}$$

If $\boldsymbol{n}$ denotes the unit normal to the boundary, then from Eq. (16), we get

$$\boldsymbol{\nabla} G\cdot\boldsymbol{n} - \frac{1}{|\boldsymbol{x}|}\left(ik + \frac{1}{|\boldsymbol{x}|}\right)(\boldsymbol{x}\cdot\boldsymbol{n}) G = |\boldsymbol{x}| \, e^{ik|\boldsymbol{x}|}(\boldsymbol{\nabla}\tilde{p}\cdot\boldsymbol{n}). \tag{19}$$

The variational formulation for $G$ is obtained by multiplying Eq. (18) by the variation $G_\delta$ and carrying out an appropriate

integration by parts. We get

$$\int_\Omega \left[\boldsymbol{\nabla} G_\delta \cdot \boldsymbol{\nabla} G + \frac{2}{|\boldsymbol{x}|} G_\delta \left(ik + \frac{1}{|\boldsymbol{x}|}\right) \boldsymbol{\nabla} G \cdot \boldsymbol{x}\right] d\Omega = \int_\Gamma G_\delta \boldsymbol{\nabla} G \cdot \boldsymbol{n}\, d\Gamma. \quad (20)$$

Substituting Eq. (19) into Eq. (20), we get

$$\int_\Omega \left[\boldsymbol{\nabla} G_\delta \cdot \boldsymbol{\nabla} G + \frac{2}{|\boldsymbol{x}|} G_\delta \left(ik + \frac{1}{|\boldsymbol{x}|}\right) \boldsymbol{\nabla} G \cdot \boldsymbol{x}\right] d\Omega - \int_\Gamma \frac{1}{|\boldsymbol{x}|} G_\delta \left(ik + \frac{1}{|\boldsymbol{x}|}\right) (\boldsymbol{x} \cdot \boldsymbol{n}) G\, d\Gamma = \int_\Gamma G_\delta\, |\boldsymbol{x}|\, e^{ik|\boldsymbol{x}|} (\boldsymbol{\nabla} \tilde{p} \cdot \boldsymbol{n})\, d\Gamma. \quad (21)$$

On the radiating surface $\Gamma_r$, $\boldsymbol{\nabla}\tilde{p} \cdot \boldsymbol{n}$ is as given by Eq. (4a), while on $\Gamma_\infty$, by using Eq. (6) and (15), we have $\boldsymbol{\nabla} G \cdot \boldsymbol{n} = 0$; thus, similar to the PML, no boundary condition needs to be imposed on $\Gamma_\infty$. It follows that, for a radiation problem, Eq. (21) can be written as

$$\int_\Omega \left[\boldsymbol{\nabla} G_\delta \cdot \boldsymbol{\nabla} G + \frac{2}{|\boldsymbol{x}|} G_\delta \left(ik + \frac{1}{|\boldsymbol{x}|}\right) \boldsymbol{\nabla} G \cdot \boldsymbol{x}\right] d\Omega - \int_{\Gamma_r} \frac{1}{|\boldsymbol{x}|} G_\delta \left(ik + \frac{1}{|\boldsymbol{x}|}\right) (\boldsymbol{x} \cdot \boldsymbol{n}) G\, d\Gamma = -\int_{\Gamma_r} G_\delta\, |\boldsymbol{x}|\, e^{ik|\boldsymbol{x}|} \rho_f i\omega v_n\, d\Gamma. \quad (22)$$

Note that on the surface $\Gamma_r$, the term $e^{ik|\boldsymbol{x}|}$ does not vary rapidly (e.g., if $\Gamma_r$ is a sphere, then it is a constant), and hence standard Gaussian quadrature can be used. Note also that on symmetry surfaces in the finite element model where $\boldsymbol{\nabla}\tilde{p} \cdot \boldsymbol{n} = 0$, since $\boldsymbol{x} \cdot \boldsymbol{n} = 0$, it follows from Eq. (19) that $\boldsymbol{\nabla} G \cdot \boldsymbol{n}$ is also zero.

The finite element formulation is obtained by discretizing $G$ using the same interpolations as used for $\tilde{p}$ in Eq. (7), i.e.,

$$G = \boldsymbol{N}_p \hat{\boldsymbol{g}}, \qquad G_\delta = \boldsymbol{N}_p \hat{\boldsymbol{g}}_\delta; \quad (23a)$$

$$\boldsymbol{\nabla} G = \boldsymbol{B}_p \hat{\boldsymbol{g}}, \qquad \boldsymbol{\nabla} G_\delta = \boldsymbol{B}_p \hat{\boldsymbol{g}}_\delta, \quad (23b)$$

with $\boldsymbol{B}_p$ given by Eq. (8). Substituting these interpolations into Eq. (22), and using the arbitrariness of $\hat{\boldsymbol{g}}_\delta$, we get the finite element matrix equation as

$$[\boldsymbol{K}_g + i\omega \boldsymbol{C}_g]\, \hat{\boldsymbol{g}} = \hat{\boldsymbol{f}}_g; \quad (24)$$

where

$$\boldsymbol{K}_g = \int_\Omega \left[\boldsymbol{B}_p^T \boldsymbol{B}_p + \frac{2}{|\boldsymbol{x}|^2} \boldsymbol{N}_p^T \boldsymbol{x}^T \boldsymbol{B}_p\right] d\Omega - \int_{\Gamma_r} \frac{\boldsymbol{x} \cdot \boldsymbol{n}}{|\boldsymbol{x}|^2} \boldsymbol{N}_p^T \boldsymbol{N}_p\, d\Gamma; \quad (25)$$

$$\boldsymbol{C}_g = \int_\Omega \frac{2}{c\,|\boldsymbol{x}|} \boldsymbol{N}_p^T \boldsymbol{x}^T \boldsymbol{B}_p\, d\Omega - \int_{\Gamma_r} \frac{\boldsymbol{x} \cdot \boldsymbol{n}}{c\,|\boldsymbol{x}|} \boldsymbol{N}_p^T \boldsymbol{N}_p\, d\Gamma; \quad (26)$$

$$\hat{\boldsymbol{f}}_g = -\int_{\Gamma_r} \rho_f i\omega v_n\, |\boldsymbol{x}|\, e^{ik|\boldsymbol{x}|} \boldsymbol{N}_p^T\, d\Gamma. \quad (27)$$

Comparing Eq. (24) with Eq. (9), we see that in the proposed formulation, the $\boldsymbol{M}_p$ matrix is absent, while the damping terms are due to integrals over the domain $\Omega$ and boundary $\Gamma_r$ instead of over $\Gamma_\infty$. In addition, because outgoing waves are favoured, the matrices are also unsymmetric. However, since the matrices are still sparse, it does not result in a significant increase in computational cost. Once $\hat{\boldsymbol{g}}$ is determined, the pressure field is recovered using Eq. (15).

In the case of scattering by a rigid body, we approximate the scattered field $p_{\text{scat}}$ as $G(\boldsymbol{x}) e^{-ik|\boldsymbol{x}|} / |\boldsymbol{x}|$ so that we end up with the same equation as Eq. (24) with $\Gamma_s$ in the place of $\Gamma_r$, and the load vector, when the incident wave is as given by Eq. (5), now given by

$$\hat{\boldsymbol{f}}_g = -\int_{\Gamma_s} p_i i(\boldsymbol{k} \cdot \boldsymbol{n})\, |\boldsymbol{x}|\, e^{i(\boldsymbol{k}\cdot\boldsymbol{x} + k|\boldsymbol{x}|)} \boldsymbol{N}_p^T\, d\Gamma.$$

When the origin is part of the acoustical domain (e.g., radiation from a circular plate in a baffle), we use conventional elements in the region between the radiator (or scatterer) and a sphere $\Gamma_1$ whose radius is denoted by $r_1$, and the proposed elements in the region between $\Gamma_1$ and $\Gamma_\infty$. In order to ensure continuity of the pressure field at the interface $\Gamma_1$, we modify Eq. (15) to

$$\tilde{p} = \frac{r_1}{|\boldsymbol{x}|} G(\boldsymbol{x}) e^{ik(r_1 - |\boldsymbol{x}|)}. \quad (28)$$

The matrix formulation presented in Eq. (24) remains unaltered because of this scaling by a constant—the only difference being that one multiplies the expression for $\hat{\boldsymbol{f}}_g$ by $e^{-ikr_1}/r_1$, and one uses Eq. (28) instead of Eq. (15) while recovering the actual pressure field from $G(\boldsymbol{x})$. The matrix formulation for the conventional formulation also remains unaltered except that matrices that are evaluated over $\Gamma_\infty$ are now evaluated over $\Gamma_1$, ensuring continuity of $\boldsymbol{\nabla}\tilde{p} \cdot \boldsymbol{n}$ (in a weak sense) between the two types of elements.

It may appear that an approximation of the type $\tilde{p} = G(\boldsymbol{x}) e^{-ik|\boldsymbol{x}|}$ may bypass the use of conventional elements altogether, even when the origin is part of the acoustic domain; however, numerical experiments show that the results are poor in the vicinity of the origin since $\boldsymbol{\nabla}\tilde{p}$ has a term $\boldsymbol{x}/|\boldsymbol{x}|$ that becomes indeterminate at the origin, leading to ill-conditioning. The second-order damper presented in the work of Bossut and Decarpigny[22] was also tried both with this approximation and the conventional formulation, but resulted only in a marginal improvement, especially since I ensured that $R$ is chosen such that $kR \gg 1$.

In the wave-envelope method of Astley and Eversman[17,18] one substitutes

$$\tilde{p} = \frac{1}{|\boldsymbol{x}|} G(\boldsymbol{x}) e^{-ik|\boldsymbol{x}|}; \quad p_\delta = \frac{1}{|\boldsymbol{x}|} G_\delta(\boldsymbol{x}) e^{ik|\boldsymbol{x}|}; \quad (29)$$

into the conventional variational formulation given by Eq. (3). The result is equations of the same form as Eq. (24), but with different $\boldsymbol{K}_g$, $\boldsymbol{C}_g$ and $\hat{\boldsymbol{f}}_g$ matrices as given by

$$\boldsymbol{K}_g = \int_\Omega \tfrac{1}{|\boldsymbol{x}|^2} \left[\boldsymbol{B}_p^T \boldsymbol{B}_p + \tfrac{1}{|\boldsymbol{x}|^2} \begin{pmatrix} \boldsymbol{N}_p^T \boldsymbol{N}_p - \boldsymbol{N}_p^T \boldsymbol{x}^T \boldsymbol{B}_p \\ -\boldsymbol{B}_p^T \boldsymbol{x} \boldsymbol{N}_p \end{pmatrix}\right] d\Omega + \int_{\Gamma_\infty} \tfrac{1}{|\boldsymbol{x}|^3} \boldsymbol{N}_p^T \boldsymbol{N}_p\, d\Gamma; \quad (30)$$

$$\boldsymbol{C}_g = \int_\Omega \frac{1}{c\,|\boldsymbol{x}|^3}\left[\boldsymbol{N}_p^T\boldsymbol{x}^T\boldsymbol{B}_p - \boldsymbol{B}_p^T\boldsymbol{x}\boldsymbol{N}_p\right] d\Omega + \int_{\Gamma_\infty} \frac{1}{c\,|\boldsymbol{x}|^2}\boldsymbol{N}_p^T\boldsymbol{N}_p\, d\Gamma; \quad (31)$$

$$\hat{\boldsymbol{f}}_g = -\int_{\Gamma_r} \frac{1}{|\boldsymbol{x}|}\rho_f i\omega v_n e^{ik|\boldsymbol{x}|}\boldsymbol{N}_p^T\, d\Gamma. \quad (32)$$

When used in conjunction with conventional elements, one again uses Eq. (28) for the pressure and its complex conjugate for the variation so that one multiplies the above $\boldsymbol{K}_g$, $\boldsymbol{C}_g$ by $r_1^2$ and $\hat{\boldsymbol{f}}_g$ by $r_1/e^{ikr_1}$. Since the weak continuity of $\boldsymbol{\nabla}\tilde{p}\cdot\boldsymbol{n}$ is automatically satisfied, no boundary condition needs to be imposed at $\Gamma_1$. Note the following:

1. The derivation of the above wave envelope elements has been carried out using the same critical idea of replacing $r$ by $|\boldsymbol{x}|$ as used for the proposed method and thus leads to the same advantage of being able to replace conventional elements in most problems. In line with the equivalence shown between these two approaches for some one-dimensional problems with piecewise-linear shape functions,[23] the results obtained using the above approach are very similar to the results obtained using the proposed formulation. (Note, however, that the matrix expressions as given by Eqs. (25)–(27) are not only more compact, and hence more economical to compute, but are also simpler to implement since they do not involve any integrals over $\Gamma_\infty$) The original wave envelope formulation[17,18] is, however, based on a separation of the shape functions into radial and angular directions necessitating the use of an inner mesh of conventional elements and leading to poorer accuracy, as shown in section 4.

2. The radial direction is treated in a special manner even in recent enhancements of the wave envelope formulation in the literature, and other complications are involved, such as the need to choose weighting functions for these elements and the location of virtual source nodes; for example, see the rather involved way of constructing the radial shape functions as discussed in section IIC of Astley et al.,[20] or as discussed by Cremers and Fyfe,[24] the difficulties associated with identifying the source location for radiators of arbitrary shape, which can lead to large meshes of conventional elements. Again, in contrast, in this formulation, the radial direction is not treated in a special manner, since the oscillatory terms associated with the radial direction have already been eliminated a priori (thus, we use standard Lagrange shape functions). And since they are similar to conventional elements, no factors need to be adjusted, no weights need to be chosen, and no virtual source nodes need to be identified.

## 3. COUPLED FORMULATION

I first briefly present the so-called pressure formulation[25] for coupled problems within the conventional setup and then present a formulation analogous to this pressure formulation for the proposed method. Assume that three-dimensional elements, such as tetrahedral or hexahedral elements, are used to conduct the structural analysis. If $\hat{\boldsymbol{u}}$ denotes the vector of the displacement degrees of freedom,

$$\boldsymbol{N}_u = \begin{bmatrix} N_1 & 0 & 0 & N_2 & 0 & 0 & \dots \\ 0 & N_1 & 0 & 0 & N_2 & 0 & \dots \\ 0 & 0 & N_1 & 0 & 0 & N_2 & \dots \end{bmatrix}; \quad (33)$$

denotes the shape function matrix (i.e., $\boldsymbol{u} = \boldsymbol{N}_u\hat{\boldsymbol{u}}$); $\Gamma_{\text{wet}}$ denotes the wet surface (i.e., the interface between the structure and the acoustic fluid); $\boldsymbol{n}$ denotes the unit normal to the surface; and $\boldsymbol{K}_s$, $\boldsymbol{M}_s$, and $\boldsymbol{C}_s$ denote the stiffness, mass, and damping matrices for the structure, then the matrix equations for a radiation problem can be written as

$$\begin{bmatrix} \boldsymbol{K}_{uu} & \boldsymbol{K}_{up} \\ \boldsymbol{K}_{pu} & \boldsymbol{K}_{pp} \end{bmatrix}\begin{bmatrix} \hat{\boldsymbol{u}} \\ \hat{\boldsymbol{p}} \end{bmatrix} = \begin{bmatrix} \hat{\boldsymbol{f}}_u \\ \hat{\boldsymbol{f}}_p \end{bmatrix}; \quad (34)$$

where, with $\boldsymbol{K}_p$, $\boldsymbol{M}_p$, $\boldsymbol{C}_p$, and $\hat{\boldsymbol{f}}_p$ given by Eqs. (10)–(13),

$$\boldsymbol{K}_{uu} = \boldsymbol{K}_s - \omega^2\boldsymbol{M}_s + i\omega\boldsymbol{C}_s;$$
$$\boldsymbol{K}_{up} = \int_{\Gamma_{\text{wet}}} \boldsymbol{N}_u^T\boldsymbol{n}\boldsymbol{N}_p\, d\Gamma;$$
$$\boldsymbol{K}_{pu} = -\int_{\Gamma_{\text{wet}}} \rho_f\omega^2\boldsymbol{N}_p^T\boldsymbol{n}^T\boldsymbol{N}_u\, d\Gamma;$$
$$\boldsymbol{K}_{pp} = \boldsymbol{K}_p - \omega^2\boldsymbol{M}_p + i\omega\boldsymbol{C}_p.$$

The normal $\boldsymbol{n}$ that occurs in the expressions for $\boldsymbol{K}_{up}$ and $\boldsymbol{K}_{pu}$ represents the outward unit normal to the structural and fluid domains, respectively. The load vector $\hat{\boldsymbol{f}}_u$ is due to the external loading on the structure; for example, if a given pressure $p_s$ acts on part of the surface $\Gamma_p$, then $\hat{\boldsymbol{f}}_u = -\int_{\Gamma_p} p_s\boldsymbol{N}_u^T\boldsymbol{n}\, d\Gamma$. In the case of the scattering problem considered in the previous section, where the scattering now occurs over the wet surface $\Gamma_{\text{wet}}$, the above set of equations remains the same, with $\hat{\boldsymbol{p}}$ now denoting the nodal variables for the scattered pressure and

$$\hat{\boldsymbol{f}}_u = -\int_{\Gamma_{\text{wet}}} p_i e^{i\boldsymbol{k}\cdot\boldsymbol{x}}\boldsymbol{N}_u^T\boldsymbol{n}\, d\Gamma$$
$$\hat{\boldsymbol{f}}_p = -\int_{\Gamma_{\text{wet}}} p_i i(\boldsymbol{k}\cdot\boldsymbol{n}) e^{i\boldsymbol{k}\cdot\boldsymbol{x}}\boldsymbol{N}_p^T\, d\Gamma.$$

Similar to the uncoupled formulation in the previous section and coupled formulation above, we get the coupled equations for the proposed formulation as

$$\begin{bmatrix} \boldsymbol{K}_{uu} & \boldsymbol{K}_{ug} \\ \boldsymbol{K}_{gu} & \boldsymbol{K}_{gg} \end{bmatrix}\begin{bmatrix} \hat{\boldsymbol{u}} \\ \hat{\boldsymbol{g}} \end{bmatrix} = \begin{bmatrix} \hat{\boldsymbol{f}}_u \\ \hat{\boldsymbol{f}}_g \end{bmatrix}; \quad (35)$$

where, with $\boldsymbol{K}_g$, $\boldsymbol{C}_g$, and $\hat{\boldsymbol{f}}_g$ given by Eqs. (25)–(27),

$$\boldsymbol{K}_{uu} = \boldsymbol{K}_s - \omega^2\boldsymbol{M}_s + i\omega\boldsymbol{C}_s;$$
$$\boldsymbol{K}_{ug} = \int_{\Gamma_{\text{wet}}} \frac{1}{|\boldsymbol{x}|}e^{-ik|\boldsymbol{x}|}\boldsymbol{N}_u^T\boldsymbol{n}\boldsymbol{N}_p\, d\Gamma;$$
$$\boldsymbol{K}_{gu} = -\int_{\Gamma_{\text{wet}}} \rho_f\omega^2\,|\boldsymbol{x}|\, e^{ik|\boldsymbol{x}|}\boldsymbol{N}_p^T\boldsymbol{n}^T\boldsymbol{N}_u\, d\Gamma;$$
$$\boldsymbol{K}_{gg} = \boldsymbol{K}_g + i\omega\boldsymbol{C}_g - \int_{\Gamma_{\text{wet}}} \frac{\boldsymbol{x}\cdot\boldsymbol{n}}{|\boldsymbol{x}|}\left(ik + \frac{1}{|\boldsymbol{x}|}\right)\boldsymbol{N}_p^T\boldsymbol{N}_p\, d\Gamma.$$

The load vector $\hat{\boldsymbol{f}}_u$ is as in the conventional formulation above for both the radiation and scattering problems. For the scattering problem,

$$\hat{\boldsymbol{f}}_g = -\int_{\Gamma_{\text{wet}}} p_i i(\boldsymbol{k}\cdot\boldsymbol{n})\,|\boldsymbol{x}|\,e^{i\boldsymbol{k}\cdot\boldsymbol{x}+ik|\boldsymbol{x}|}\boldsymbol{N}_p^T\,d\Gamma.$$

As in the uncoupled case, once $\hat{\boldsymbol{g}}$ is found, $\tilde{p}$ is recovered using Eq. (15). Thus, the great simplicity of formulation and implementation inherent in the uncoupled case carries over to the coupled problem.

For both the coupled and uncoupled problems presented above, an axisymmetric formulation can be developed easily from the three-dimensional formulation. If $(r, z)$ represent the coordinates in the cylindrical coordinate system and $\xi$ represents the natural coordinate parametrizing the boundary in the finite element framework, then the normal and the area element are given by

$$\boldsymbol{n} = \left(\frac{dz/d\xi}{\sqrt{(dr/d\xi)^2+(dz/d\xi)^2}}, -\frac{dr/d\xi}{\sqrt{(dr/d\xi)^2+(dz/d\xi)^2}}\right);$$

$$d\Gamma = 2\pi r\sqrt{\left(\frac{dr}{d\xi}\right)^2+\left(\frac{dz}{d\xi}\right)^2}\,d\xi;$$

while the $\boldsymbol{B}_p$ and $\boldsymbol{N}_u$ matrices are obtained by a straightforward modification of Eqs. (8) and (33).

## 4. NUMERICAL EXAMPLES

I present several numerical examples, involving both radiation and scattering in the coupled and uncoupled frameworks, to illustrate the performance of the proposed method. The pressure values presented are directly the nodal values obtained from the finite element formulation, and no use is made of the Helmholtz integral equation to compute the far-field pressure, as is done in the case of some infinite elements.[9] In many examples, a high value of $R$ is deliberately chosen to show the high accuracy of the far-field pressure. The values of the input data and the corresponding results are in SI (or appropriate consistent) units.

Since the proposed method is similar to the conventional method, which uses absorbing boundary conditions (described briefly in section 2), I shall compare the proposed method with the conventional method; the similarity is borne out by the fact that both strategies use the same mesh and other input data. Wherever possible, we also carry out comparisons with other techniques such as the boundary element method, infinite element method, PML, ultra-weak variational formulation, etc. I use either 9-node axisymmetric elements or a combination of 18-node wedge and 27-node hexahedral elements in both the formulations. When used within the context of the conventional formulation, these elements are denoted by B9 and B18/B27, while they are denoted by A9 and W18/S27 when used within the context of the proposed formulation. In the coupled problems presented, standard displacement-based elements are used to conduct the structural analysis and are obviously of the same order as the acoustic elements in order to maintain compatibility with the acoustic mesh. Full integration (in both the structural and acoustic elements) and uniform meshes are used in all the examples. The Watson Sparse Matrix Package solver is used to solve the system of equations.[26,27]

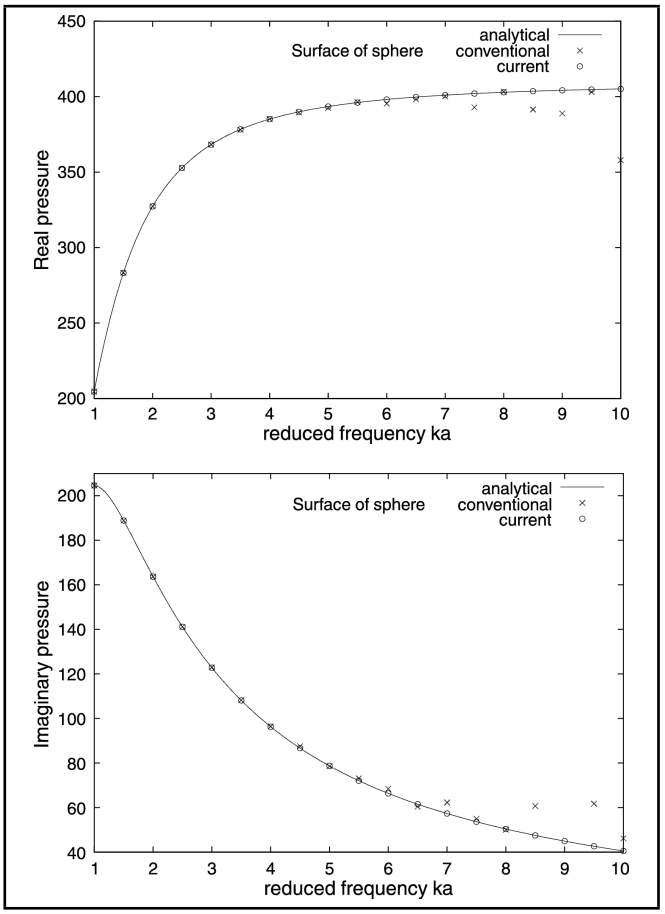


**Figure 1.** Comparison of the numerically and analytically obtained real and imaginary parts of the surface pressure for various frequencies in the pulsating sphere problem.

### 4.1. Pulsating Sphere Problem

A sphere of radius $a = 10$ vibrates with uniform radial velocity $u_0 = 1$. The analytical solution[28] for the pressure as a function of the radial distance $r$ is

$$\tilde{p}(r) = \frac{\rho_f c u_0}{r}\frac{ika^2}{1+ika}e^{-ik(r-a)}.$$

Due to symmetry, I model only half of the sphere using a uniform mesh of $16 \times 16$ axisymmetric elements (almost identical results are obtained if one solves the problem using three-dimensional elements, i.e., by discretizing one-eighth of the domain using an equivalent mesh of 18-node wedge and 27-node hexahedral elements). The bounding surface is taken to be a sphere of radius $R = 50$. The properties used are $\rho_f = 1.2$ and $c = 341$. Since $G(\boldsymbol{x})$ is a constant in this problem, the exact solution is captured by the proposed method irrespective of the mesh density and bounding radius $R$. Thus, this problem acts like a patch test for the proposed formulation.

A comparison of the real and imaginary parts of the surface and far-field pressures against the analytical solution for various frequencies of oscillation is shown in Figs. (1) and (2).

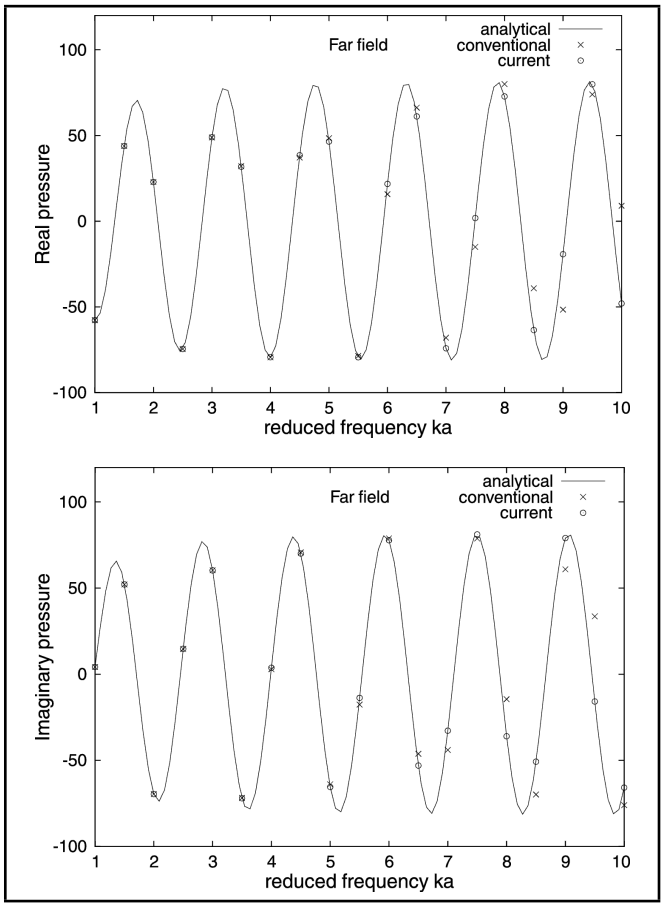


**Figure 2.** Comparison of the numerically and analytically obtained real and imaginary parts of the pressure at $r = 50$ for various frequencies in the pulsating sphere problem.

As seen from Figs. (1) and (2), although the conventional formulation yields good results at low frequencies, it results in significant errors at higher frequencies, while the proposed formulation yields very accurate results over the entire frequency range, even at points that lie on the outer bounding surface. I have also verified that the proposed formulation continues to yield the exact result, both in the near and far-field (including at $r = R$), over the entire frequency range when $R = 90$, with the same mesh density as used when $R = 50$, thus showing the insensitivity to mesh density in this particular example. In addition, one can obtain almost the exact particle velocity (which is proportional to $\boldsymbol{\nabla}\tilde{p}$) over the entire frequency range, and over the entire domain.

Huttunen et al.[13] consider the very similar problem of a point source, which is solved using the ultra-weak variational formulation combined with the PML. In spite of carrying out extensive tests to determine the optimal value of various parameters in their method and in spite of using a very fine mesh (see Huttunen et al.'s Fig. (2)), the errors in their solution are large (see Huttunen et al.'s Fig. (4)), even on this simple problem.

## 4.2. Oscillating Sphere Problem

A rigid sphere of radius $a = 10$ oscillates along the $z$-axis as shown in Fig. (3). The analytical solution[29] for the pressure as a function of the radial distance $r$ from the centre of the sphere and the angle $\theta$ between the radius vector and the

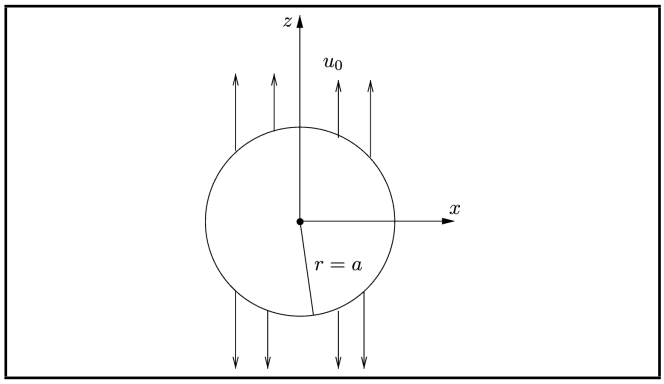


**Figure 3.** Oscillating sphere problem geometry.

velocity vector is

$$\tilde{p}(r,\theta) = \rho_f c u_0 \Big(\frac{a}{r}\Big)^2 \cos\theta \frac{ika(1+ikr)}{2(1+ika)-(ka)^2} e^{-ik(r-a)}.$$

An axisymmetric mesh of $n_r \times n_\theta = 16 \times 32$ is used to discretize the domain. The material properties and the value of $R$ are chosen to be the same as in the pulsating sphere problem, and $u_0$ is taken as unity. The solution obtained at $(0, 0, a)$ and $(0, 0, R)$ for various frequencies of oscillation is shown in Figs. (4) and (5). The high relative accuracy of the proposed formulation is again evident from these figures. Almost the same high accuracy is obtained both in the near and far-field over the entire frequency range shown, even for a much larger choice of radius of the bounding sphere, such as $R = 90$ (with the same $n_r \times n_\theta$ mesh as used for $R = 50$).

Although I have shown the results only up to $ka = 10$, the agreement with the analytical solution continues to be good, both in the near and far-field, for very large $ka$. For example, for $ka = 200$ (when there are only $0.125$ elements per wavelength), the analytical values of pressure at $r = 10$ and $r = 50$ are $(409.2, 2.046)$ and $(-36.015, -73.49)$, while the numerical values are $(409.242, 2.02)$ and $(-36.03, -73.5)$, respectively. As an illustration, the variation of the real part of the pressure (normalized using a factor of $\rho_f c u_0$) for $ka = 100$ as a function of $r/a$ at $\theta = 0$, and as a function of $\cos\theta$ at $r = a$, using the same mesh and material data mentioned above, are shown in Fig. (6); note that the conventional method fails completely at these high frequencies.

Even beyond $ka = 200$, the accuracy of the proposed formulation reduces very gradually. In contrast, with the wave envelope method of Astley, Macaulay, and Coyette,[19] there are differences between the analytical and numerical results even for as small a $ka$ value as $2\pi$ (see Astley, Macaulay, and Coyette's Fig. (9b)).

## 4.3. Radiation from an Elastic Hollow Sphere

The inner surface of an elastic hollow sphere of inner and outer radii $r_1$ and $r_2$ is loaded with a uniform time-harmonic pressure $p_0 e^{i\omega t}$. If $(\lambda, \mu)$ denote the Lame constants for the solid, and if $\rho_s$ denotes its density, then the wave number in the solid is

$$k_s = \omega\sqrt{\rho_s}/\sqrt{\lambda + 2\mu}.$$

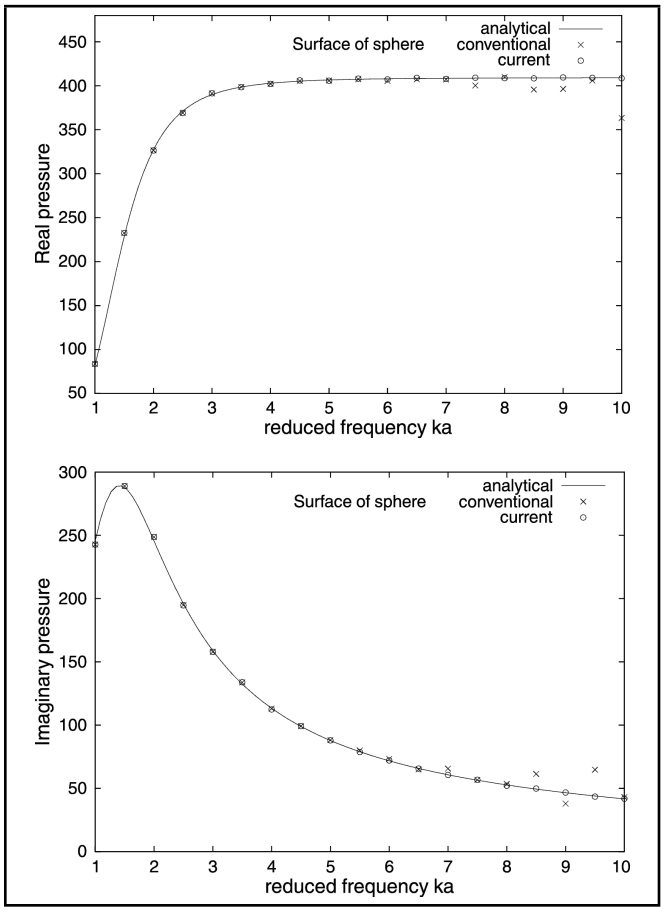


**Figure 4.** Comparison of the numerically and analytically obtained real and imaginary parts of the surface pressure for various frequencies in the oscillating sphere problem.

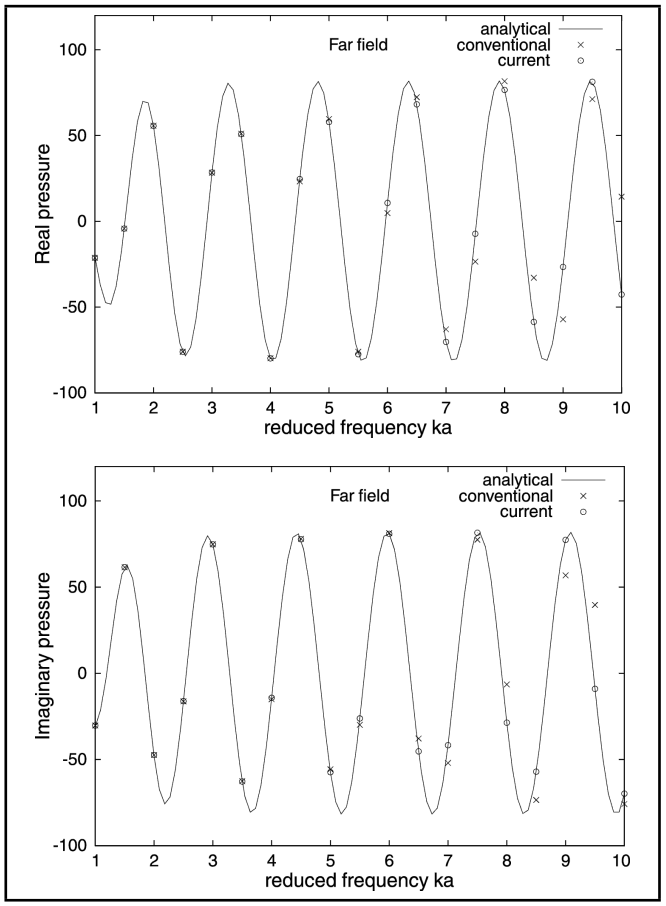


**Figure 5.** Comparison of the numerically and analytically obtained real and imaginary parts of the pressure at $r = 50$ for various frequencies in the oscillating sphere problem.

Using the approach outlined in Seybert, Wu, and Wu,[30] we find that the pressure field outside the sphere as a function of the radial coordinate $r$ is given by

$$\tilde{p} = Ne^{-ikr}/(rD);$$

where

$$N = -2e^{i(kr_2+k_s(r_1+r_2))}k_s^3(\lambda+2\mu)\omega^2 p_0 r_1^3 r_2^3 \rho_f;$$

$$D = e^{2ik_s r_1}\left[-4\mu + 4ik_s\mu r_1 + k_s^2(\lambda+2\mu)r_1^2\right]\cdot$$
$$\cdot\left[(-i+kr_2)\begin{pmatrix}-4\mu - 4ik_s\mu r_2 + \\ k_s^2(\lambda+2\mu)r_2^2\end{pmatrix} + \omega^2 r_2^2(i-k_s r_2)\rho_f\right]$$
$$- e^{2ik_s r_2}\left[-4\mu - 4ik_s\mu r_1 + k_s^2(\lambda+2\mu)r_1^2\right]\cdot$$
$$\cdot\left[(-i+kr_2)\begin{pmatrix}-4\mu + 4ik_s\mu r_2 + \\ k_s^2(\lambda+2\mu)r_2^2\end{pmatrix} + \omega^2 r_2^2(i+k_s r_2)\rho_f\right].$$

We take $r_1 = 10$ m, $r_2 = 12.5$ m, $E = 2\times10^{11}$ Pa, $\nu = 0.25$ (where $E$ and $\nu$ denote the Young modulus and Poisson ratio of the solid, respectively), $\rho_s = 7800$ kg/m$^3$, $\rho_f = 1000$ kg/m$^3$, $c = 1500$ m/s, and $p_0 = 1$ Pa (note that we have used properties for a heavy fluid where a coupled analysis is more relevant). A uniform mesh of $16\times16$ axisymmetric elements was used to mesh half the spherical domain, which comprises both the structure and the acoustic fluid (it has been verified that similar results are obtained using three-dimensional elements). The results for the pressure at the surface $r = 12.5$ m and at the bounding sphere $r = 50$ are shown in Table 1. Similar to the observation in the previous problems, the results obtained using the conventional formulation are poor at high frequencies, while the proposed formulation yields accurate results at high frequencies even in the far-field.

**Table 1.** Comparison of surface and far-field pressures in the hollow sphere radiation problem.

| $kr_1$ | B9 | A9 | Analytical |
|---|---|---|---|
| | Surface pressure ($r = 12.5$) | | |
| 5 | $0.65368 - 0.18626i$ | $0.65385 - 0.18657i$ | $0.65359 - 0.18690i$ |
| 8 | $0.01624 - 0.07858i$ | $0.01662 - 0.08122i$ | $0.01662 - 0.08122i$ |
| 10 | $0.01187 - 0.05114i$ | $0.00811 - 0.05596i$ | $0.00811 - 0.05596i$ |
| | Far-field pressure ($r = 50$) | | |
| 5 | $0.16793 - 0.02541i$ | $0.16729 - 0.03016i$ | $0.16723 - 0.03025i$ |
| 8 | $0.01943 + 0.00618i$ | $0.02070 + 0.00097i$ | $0.02070 + 0.00097i$ |
| 10 | $0.01188 - 0.00644i$ | $0.00475 - 0.01331i$ | $0.00475 - 0.01331i$ |

## 4.4. Scattering from a Rigid and Elastic Hollow Sphere

A plane wave of the form $p_i e^{ik_z z}$ is incident on a rigid sphere as shown in Fig. (7). The analytical solution[31] for the scattered pressure field is given by

$$p_{\text{scat}} = -p_i\sum_{n=0}^{\infty}(2n+1)i^n\frac{j_n'(ka)}{h_n'(ka)}h_n(kr)P_n(\cos\theta);$$

where $r$ is the (spherical) radial coordinate, $\theta$ is the angle between the $z$-axis and the radial coordinate, $j_n$ is the spherical Bessel function of the first kind, $h_n$ is the Hankel function of the second kind, $P_n$ are Legendre polynomials, and primes denote derivatives of the function.

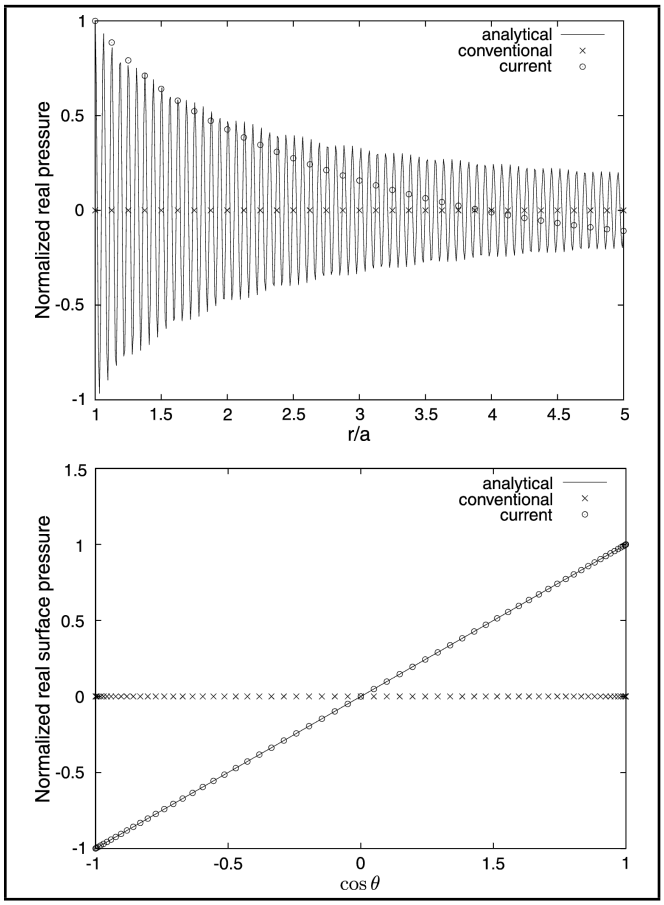


**Figure 6.** Comparison of the numerically and analytically obtained (normalized) real part of the pressure as a function of $r/a$ and $\cos\theta$, respectively, for $ka = 100$ in the oscillating sphere problem.

We take $p_i = 1$, $a = 10$, $\rho_f = 1.2$, $c = 341$, $R = 50$, and discretize the domain using an $n_r \times n_\theta = 64 \times 32$ axisymmetric mesh. The backscattered pressure on the surface and in the far-field (i.e., $p_{\text{scat}}|_{\theta=\pi}$ at $r = 10$ and $r = 50$) is tabulated in Table 2. Both the B9 and A9 elements perform equally well in this case, both in the near and far-field. The reason is that even though the $e^{-ik|\boldsymbol{x}|}$ component is present in the solution, the transverse part of the solution oscillates more rapidly than this part. Note, however, that even in such a case, the solution using the proposed strategy is no worse than the conventional one.

Now consider the case when the scattering is due to a hollow elastic sphere of inner radius $b$ and outer radius $a$. Unlike

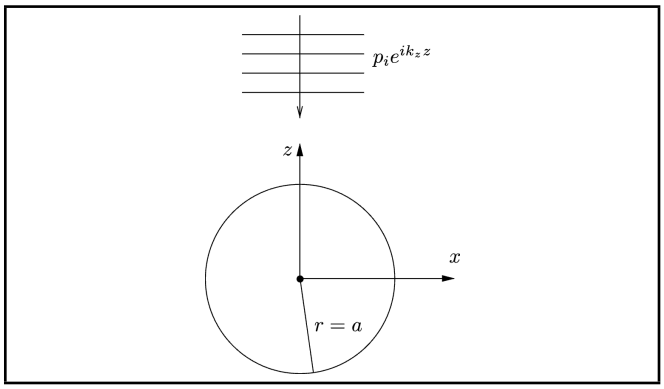


**Figure 7.** Scattering of a plane wave from a rigid sphere.

**Table 2.** Comparison of backscattered surface and far-field pressures when the sphere is rigid.

| $k_z a$ | B9 | A9 | Analytical |
|---|---|---|---|
| | Surface backscattered pressure ($r = 10$) | | |
| 1 | $-0.51049 - 0.22125i$ | $-0.51049 - 0.22125i$ | $-0.50655 - 0.22612i$ |
| 5 | $-0.54813 - 2.08572i$ | $-0.54803 - 2.08568i$ | $-0.55389 - 2.07178i$ |
| 9 | $0.42105 - 0.53238i$ | $0.41863 - 0.53435$i | $0.44242 - 0.54739i$ |
| | Far-field backscattered pressure ($r = 50$) | | |
| 1 | $0.04383 + 0.01860i$ | $0.04383 + 0.01860i$ | $0.04425 + 0.01994i$ |
| 5 | $0.11147 - 0.42893i$ | $0.11143 - 0.42893i$ | $0.11214 - 0.43208i$ |
| 9 | $-0.80695 - 0.30955i$ | $-0.80763 - 0.30765i$ | $-0.81531 - 0.31005i$ |

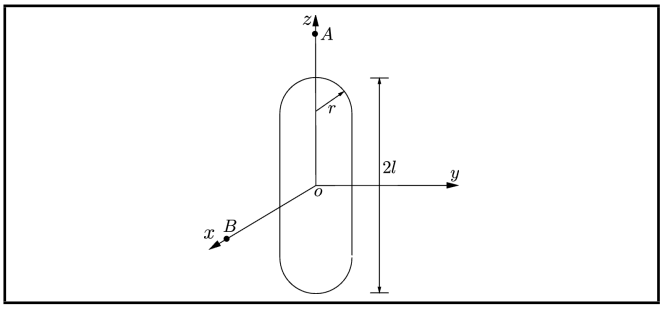


**Figure 8.** Pulsating cylinder with hemispherical end caps.

the case of the rigid sphere discussed above, this needs to be solved using the coupled formulation discussed in section 3. I use the same geometrical data and the data for hard rubber,[30] namely, $b = 0.5$ m, $a = 1$ m, $E = 2.3 \times 10^9$ Pa, $\nu = 0.4$, $\rho_s = 1100$ kg/m$^3$, $\rho_f = 1026$ kg/m$^3$, and $c = 1500$ m/s. I chose $R = 10.5$ and meshed the total domain (structure and acoustic fluid) using an $n_r \times n_\theta = 80 \times 64$ axisymmetric mesh and, in order to show the performance of the three-dimensional elements, one-fourth of the domain using an $n_r \times n_\theta \times n_\phi = 40 \times 16 \times 8$ mesh comprised of wedge and hexahedral elements. The results for various values of $k_z a$ are shown in Table 3 and compared against the values presented by Seybert, Wu, and Wu.[30] The results obtained with the conventional formulation are almost identical to the ones shown above and hence not shown again. The wedge/hexahedral mesh was deliberately chosen to be much coarser than the axisymmetric mesh to show that good results can be obtained even using a coarse mesh. Although the match with the results of Seybert, Wu, and Wu[30] is good at the lower frequencies, significant deviation at the higher frequencies occurs. I believe the reason for this deviation is that those researchers used a coarse mesh which does not capture the solution accurately at the higher frequencies; I have carried out a mesh refinement study and verified that the A9 results presented in Table 3 are close to the converged results. The accuracy of the results can also be improved further by using a mixed formulation[32] for the structural analysis rather than the displacement-based formulation that has been used in generating the above results.

## 4.5. Cylinder with Hemispherical End Caps

I consider both radiation and scattering for a problem involving a cylinder with hemispherical end caps (see Fig. (8)).[9,33,34] First I consider the radiation problem. The cylinder pulsates with a uniform normal velocity of unit magnitude over the entire surface. The dimensions used are $l = 3.5$, $r = 1$, and $R = 23.5$. For the radiation case, the fluid properties used are the same as in the pulsating sphere example. Symmetry con-

**Table 3.** Comparison of backscattered pressures at various distances when the hollow sphere is elastic; Bracketed values show the magnitude of the pressure.

| $k_z a$ | A9 | W18/S27 | $\lvert p_{\text{scat}}\rvert$ [30] |
|---|---|---|---|
| | Surface backscattered pressure ($r = 1$) | | |
| 0.2 | $-0.9437E{-}2 + 0.4911E{-}2i$ $(0.1064E{-}1)$ | $-0.9462E{-}2 + 0.4917E{-}2i$ $(0.1066E{-}1)$ | $0.1063E{-}1$ |
| 0.4 | $-0.4414E{-}1 + 0.1349E{-}1i$ $(0.4615E{-}1)$ | $-0.4418E{-}1 + 0.1358E{-}1i$ $(0.4620E{-}1)$ | $0.4606E{-}1$ |
| 0.6 | $-0.1452E0 + 0.2999E{-}1i$ $(0.1483E0)$ | $-0.1447E0 + 0.3010E{-}1i$ $(0.1478E0)$ | $0.1455E0$ |
| 0.8 | $-0.8658E0 + 0.8683E{-}1i$ $(0.8701E0)$ | $-0.8425E0 + 0.8540E{-}1i$ $(0.8468E0)$ | $0.7441E0$ |
| 1.0 | $0.6857E0 + 0.1250E0i$ $(0.6970E0)$ | $0.6990E0 + 0.1256E0i$ $(0.7102E0)$ | $0.7419E0$ |
| | Backscattered pressure at $r = 3$ | | |
| 0.2 | $-0.3641E{-}3 + 0.5893E{-}3i$ $(0.6927E{-}3)$ | $-0.3726E{-}3 + 0.5952E{-}3i$ $(0.7023E{-}3)$ | $0.7039E{-}3$ |
| 0.4 | $-0.1571E{-}2 + 0.1700E{-}2i$ $(0.2315E{-}2)$ | $-0.1583E{-}2 + 0.1739E{-}2i$ $(0.2352E{-}2)$ | $0.2959E{-}3$ |
| 0.6 | $-0.6828E{-}2 + 0.4254E{-}2i$ $(0.8045E{-}2)$ | $-0.6764E{-}2 + 0.4337E{-}2i$ $(0.8035E{-}2)$ | $0.1118E{-}1$ |
| 0.8 | $-0.6228E{-}1 + 0.3689E{-}1i$ $(0.7238E{-}1)$ | $-0.6039E{-}1 + 0.3599E{-}1i$ $(0.7030E{-}1)$ | $0.6783E{-}1$ |
| 1.0 | $0.5645E{-}1 - 0.5132E{-}1i$ $(0.7629E{-}1)$ | $0.5780E{-}1 - 0.5238E{-}1i$ $(0.7800E{-}1)$ | $0.7248E{-}1$ |
| | Backscattered pressure at $r = 10$ | | |
| 0.2 | $0.6466E{-}4 + 0.6618E{-}4i$ $(0.9253E{-}4)$ | $0.6599E{-}4 + 0.6905E{-}4i$ $(0.9551E{-}4)$ | $0.9751E{-}4$ |
| 0.4 | $0.1900E{-}3 - 0.1308E{-}3i$ $(0.2307E{-}3)$ | $0.1983E{-}3 - 0.1407E{-}3i$ $(0.2432E{-}3)$ | $0.5866E{-}3$ |
| 0.6 | $0.9077E{-}3 - 0.4914E{-}3i$ $(0.1032E{-}2)$ | $0.8723E{-}3 - 0.4973E{-}3i$ $(0.1004E{-}2)$ | $0.2597E{-}2$ |
| 0.8 | $-0.7941E{-}2 - 0.1353E{-}1i$ $(0.1569E{-}1)$ | $-0.7698E{-}2 - 0.1309E{-}1i$ $(0.1519E{-}1)$ | $0.1647E{-}1$ |
| 1.0 | $0.1315E{-}1 - 0.1402E{-}1i$ $(0.1922E{-}1)$ | $0.1349E{-}1 - 0.1435E{-}1i$ $(0.1969E{-}1)$ | $0.1698E{-}1$ |

**Table 4.** Comparison of pressures at points A and B in the pulsating cylinder with hemispherical caps problem.

| $\omega$ | B9 | A9 | B18/B27 | W18/S27 | Bhandakkar and Jog[9] |
|---|---|---|---|---|---|
| | | | Pressure at A | | |
| 62.83 | $24.409 - 4.899i$ | $24.416 - 4.902i$ | $24.409 - 4.899i$ | $24.416 - 4.902i$ | $24.457 - 4.917i$ |
| 157.08 | $-36.716 - 14.800i$ | $-36.726 - 14.797i$ | $-36.716 - 14.799i$ | $-36.726 - 14.797i$ | $-36.391 - 14.809i$ |
| 318.03 | $11.010 + 14.170i$ | $10.968 + 14.117i$ | $11.010 + 14.169i$ | $10.968 + 14.117i$ | $11.13 + 14.04i$ |
| 475.66 | $-28.154 - 27.635i$ | $-28.251 - 27.688i$ | $-28.157 - 27.633i$ | $-28.251 - 27.687i$ | $-28.392 - 27.061i$ |
| | | | Pressure at B | | |
| 66.06 | $24.373 - 9.955i$ | $24.380 - 9.959i$ | $24.373 - 9.955i$ | $24.380 - 9.959i$ | $24.157 - 8.035i$ |
| 157.94 | $-55.500 - 6.130i$ | $-55.522 - 6.121i$ | $-55.500 - 6.130i$ | $-55.522 - 6.121i$ | $-55.622 - 6.110i$ |
| 315.38 | $36.407 - 85.483i$ | $35.938 - 85.767i$ | $36.407 - 85.483i$ | $35.938 - 85.767i$ | $36.002 - 85.528i$ |
| 472.26 | $76.511 + 83.703i$ | $80.274 + 80.448i$ | $76.511 + 83.702i$ | $80.274 + 80.448i$ | $79.592 + 80.361i$ |

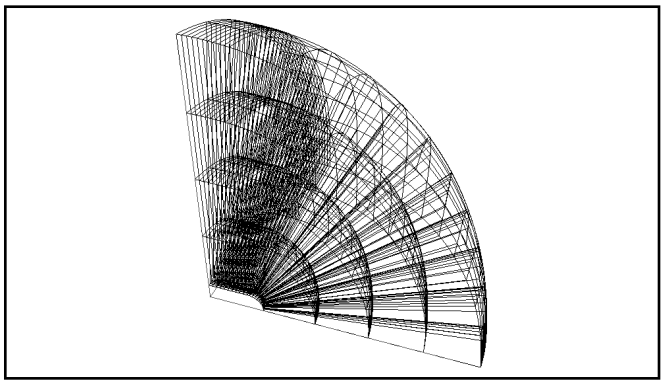

**Figure 9.** A typical mesh for the cylinder with hemispherical end caps problem; for clarity, fewer elements are shown in the radial direction than actually used.

siderations allow us to model one-eighth of the structure. A mesh of $n_r \times n_\theta \times n_\phi = 20 \times 20 \times 10$ (where $\phi$ is the circumferential direction) was used to model one-eighth of the structure as shown in Fig. (9). Solutions were also obtained using an axisymmetric mesh of $n_r \times n_\theta = 20 \times 20$ (roughly four elements per wavelength). The solutions at points A and B with coordinates $(0, 0, 10)$ and $(10, 0, 0)$, respectively, compared against the solutions in Bhandakkar and Jog,[9] are presented in Table 4. Note that the solutions presented with our strategy are the raw nodal values, while the ones in Bhandakkar and Jog[9] have been obtained using the Helmholtz integral equation. The proposed method yields a better approximation at point B at the highest frequency considered. The coarse mesh results obtained by using a $n_r \times n_\theta \times n_\phi = 8 \times 20 \times 10$ mesh and $R = 16.5$ are shown in Table 5, demonstrating the better accuracy of the proposed formulation, especially at higher frequencies.

Now I consider the scattering by the same cylinder of a plane wave that is incident along the $x$-axis and given by $e^{ik_x x}$. The fluid properties used are $\rho_f = 1026\ \text{kg/m}^3$ and $c = 1500$ m/s.

**Table 5.** Comparison of coarse-mesh pressures at point A in the pulsating cylinder with hemispherical caps problem.

| $\omega$ | B18/B27 | W18/S27 | Bhandakkar and Jog[9] |
|---|---|---|---|
| 62.83 | $24.459 - 5.036i$ | $24.498 - 5.055i$ | $24.457 - 4.917i$ |
| 157.08 | $-37.052 - 14.795i$ | $-37.139 - 14.755i$ | $-36.391 - 14.809i$ |
| 318.03 | $10.606 + 14.704i$ | $10.916 + 13.988i$ | $11.13 + 14.04i$ |
| 475.66 | $-22.997 - 31.793i$ | $-28.839 - 27.975i$ | $-28.392 - 27.061i$ |

**Table 6.** Comparison of scattered pressures at points B and C in the cylinder with hemispherical caps problem; Bracketed values show the magnitude of the pressure.

| $k_x a$ | B18/B27 | W18/S27 |
|---|---|---|
| | Pressure at B | |
| 1.5 | $1.809E{-}2 + 0.161i$ (0.162) | $2.721E{-}2 + 0.160i$ (0.162) |
| 2.25 | $-4.177E{-}2 + 0.232i$ (0.235) | $3.831E{-}2 + 0.242i$ (0.245) |
| 3 | $-0.109 - 0.242i$ (0.265) | $-3.137E{-}2 + 0.266i$ (0.268) |
| | Pressure at C | |
| 1.5 | $-0.187 + 0.122i$ (0.223) | -0.181+0.131i (0.223) |
| 2.25 | $6.994E{-}2 + 0.337i$ (0.344) | 0.182+0.313i (0.361) |
| 3 | $-0.122 + 0.273i$ (0.299) | 0.463-0.185i (0.498) |

The discretization used is similar to that in the radiation case, with a mesh of $n_r \times n_\theta \times n_\phi = 20 \times 20 \times 20$ used to mesh one-fourth of the domain. The results for the forward and backscattered pressures at points B and C with coordinates $(10, 0, 0)$ and $(-10, 0, 0)$, respectively, are presented in Table 6 ($a = 1$), and when compared against Fig. (12) of Chen and Liu,[34] again show the high accuracy of the proposed formulation.

## 4.6. Vibrating Circular Piston in a Baffle

A circular piston of radius $a = 10$ centred at the origin vibrates with a normal velocity $v_n$. The analytical expression for the pressure field[35] at a point $(0, 0, z)$ along the axis is given by

$$\tilde{p} = \rho_f c v_n \left( e^{-ik\sqrt{a^2+z^2}} - e^{-ikz} \right).$$

The properties used are $\rho_f = 1.2$ and $c = 341$. The variables $v_n$ and $R$ were chosen to be 1 and 50, respectively. A uniform mesh of $n_r \times n_\theta = 40 \times 32$ axisymmetric elements

**Table 7.** Comparison of surface and far-field pressures along the axis for the circular piston example.

| $ka$ | B6/B9 | B6/B9/A9 | Analytical |
|---|---|---|---|
| | Pressure at $z = 0$ | | |
| 1 | $188.109 + 344.338i$ | $188.109 + 344.338i$ | $188.108 + 344.330i$ |
| 5 | $293.389 - 391.894i$ | $293.413 - 391.924i$ | $293.125 - 392.392i$ |
| 10 | $761.414 - 217.362i$ | $762.958 - 215.072i$ | $752.548 - 222.613i$ |
| | Pressure at $z = 50$ | | |
| 1 | $-38.206 + 13.090i$ | $-38.206 + 13.090i$ | $-38.222 + 13.397i$ |
| 5 | $22.840 + 198.795i$ | $23.12 + 198.831i$ | $22.972 + 199.211i$ |
| 10 | $68.789 + 380.338i$ | $85.709 + 376.840i$ | $88.500 + 378.631i$ |

was used to discretize the domain with conventional triangular six-noded elements, denoted by B6, used in the layer closest to the origin. I use conventional elements up to $r_1 = 10$, and the proposed elements beyond $r_1$ and the results are compared against a mesh comprised of conventional elements alone; see Table 7. Not surprisingly, the near-field accuracy is almost the same, while the far-field accuracy is better with the proposed formulation.

To show that good far-field results are obtained even at high frequencies, I take $R = 80$ and $ka = 8\pi$, with the other properties the same as above. A uniform mesh of $n_r \times n_\theta = 120 \times 64$ axisymmetric elements is used to discretize the domain. In order to compare the results with Fig. (7.4.2) of Kinsler et al.,[28] one must normalize the pressures by a factor of $2\rho_f c v_n$. The results are shown in Fig. (10). From the plot of the absolute pressure, it may appear that the errors in the conventional formulation are small. However, in reality, the significant errors in the real and the imaginary parts of the conventional formulation, especially in the far field, cancel each other as seen from the plot for the real value of the pressure.

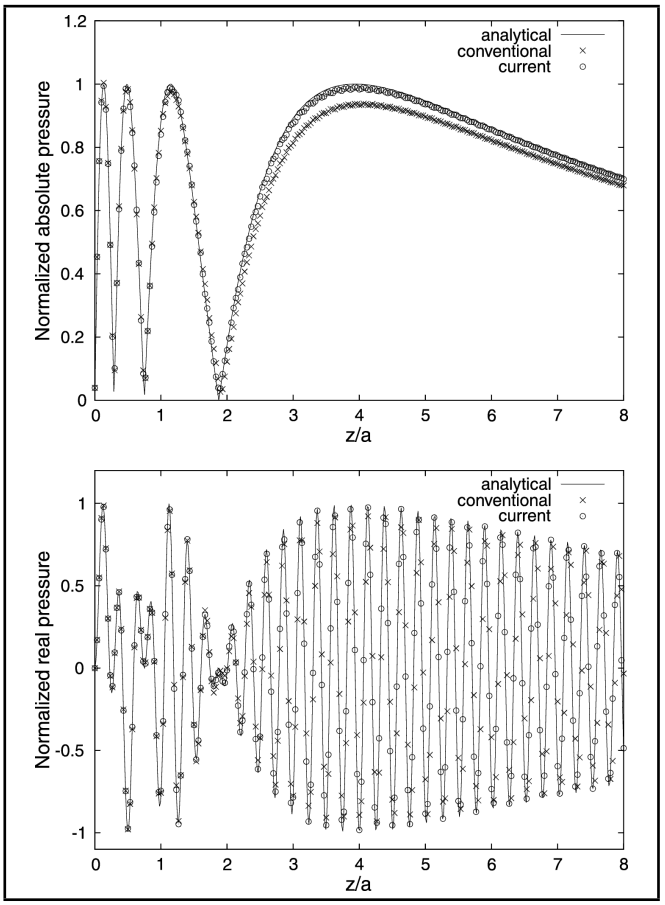


**Figure 10.** Comparison of the numerically and analytically obtained normalized pressures $|\tilde{p}|\,/(2\rho_f c v_n)$ and $\tilde{p}_r/(2\rho_f c v_n)$ along the axis of the piston as a function of $z/a$ for $ka = 8\pi$.

## 5. CONCLUSIONS

A finite element method has been proposed for exterior acoustic problems that favours outgoing waves and hence provides higher accuracy both in the near and far-field compared to other methods based on absorbing boundary conditions. The computational domain and input data are the same as for the conventional method (i.e., no extra variables are introduced). In addition, the cost of constructing the element stiffness matrix is also almost the same. Although the resulting global matrix as given in Eq. (24) is unsymmetric, it is sparse so that the computational cost is not increased significantly. The proposed elements, similar to standard finite elements, are based on Cartesian coordinates, use standard Gaussian quadrature and Lagrange interpolations, and, hence barring a few situations, can be used even in the direct vicinity of the radiator or scatterer, thereby circumventing the need of using an inner mesh of conventional elements. The method is similar to the PML method in that each layer surrounding the radiator or scatterer absorbs acoustic radiation so that no boundary condition on the truncated boundary needs to be imposed.

## Bibliography


[1] Givoli, D. Non-reflecting boundary conditions, *Journal of Computational Physics*, **94**, 1–29, (1991).

[2] Qi, Q. and Geers, T. L. Evaluation of the perfectly matched layer for computational acoustics, *Journal of Computational Physics*, **139**, 166–183, (1998).

[3] Burnett, D. S. A three-dimensional acoustic infinite element based on a prolate spheroidal multipole expansion, *Journal of the Acoustical Society of America*, **96** (5), 2798–2816, (1994).

[4] Burnett, D. S. and Holford, R. L. Prolate and oblate spheroidal acoustic infinite elements, *Computer Methods in Applied Mechanics and Engineering*, **158**, 117–142, (1998).

[5] Burnett, D. S. and Holford, R. L. An ellipsoidal acoustic infinite element, *Computer Methods in Applied Mechanics and Engineering*, **164**, 49–76, (1998).

[6] Gerdes, K. A review of infinite element methods for exterior Helmholtz problems, *Journal of Computational Acoustics*, **8** (1), 43–62, (2000).

[7] Astley, R. J. Infinite elements for wave problems: a review of current formulations and an assessment of accuracy, *International Journal for Numerical Methods in Engineering*, **49**, 951–976, (2000).

[8] Astley, R. J. and Coyette, J. P. The performance of spheroidal infinite elements, *International Journal for Numerical Methods in Engineering*, **52**, 1379–1396, (2001).

[9] Bhandakkar, T. K, and Jog, C. S. An alternative implementation of the Burnett family of acoustic finite elements, *Journal of the Acoustical Society of America*, **118** (4), 2295–2301, (2005).

[10] Dreyer, D. and Estorff, O. Improved conditioning of infinite elements for exterior acoustics, *International Journal for Numerical Methods in Engineering*, **58**, 933–953, (2003).

[11] Harari, I. A survey of finite element methods for time-harmonic acoustics, *Computer Methods in Applied Mechanics and Engineering*, **195**, 1594–1607, (2006).

[12] Shirron, J. J. and Giddings, T. E. A finite element model for acoustic scattering from objects near a fluid-fluid interface, *Computer Methods in Applied Mechanics and Engineering*, **196**, 279–288, (2006).

[13] Huttunen, T. H., Kaipio, J. P., and Monk, P. The perfectly matched layer for the ultra weak variational formulation of the 3D Helmholtz equation, *International Journal for Numerical Methods in Engineering*, **61**, 1072–1092, ( 2004).

[14] Bayliss, A. and Turkel, E. Radiation boundary conditions for wave-like equations, *Comm. Pure and Appl. Math.*, **XXXIII**, 707–725, (1980).

[15] Astley, R. J. Infinite elements, In Marburg, S. and Nolte, B. Editors, *Computational acoustics of noise propagation in fluids*, Springer, (2008).

[16] Atkinson, F. V. On Sommerfeld's radiation condition, *Philosophical Magazine*, **40**, 645–651, (1949).

[17] Astley, R. J. Wave envelope and infinite elements for acoustical radiation, *International Journal for Numerical Methods in Fluids*, **3**, 507–526, (1983).

[18] Astley, R. J. and Eversman, W. Finite element formulations for acoustical radiation, *Journal of Sound and Vibration*, **88**, 47–64, (1983).

[19] Astley, R. J., Macaulay, G. J., and Coyette J. P. Mapped wave envelope elements for acoustical radiation and scattering, *Journal of Sound and Vibration*, **170**, 97–118, (1994).

[20] Astley, R. J., Macaulay, G. J., Coyette, J. P., and Cremers L. Three-dimensional wave-envelope elements of variable order for acoustic radiation and scattering. Part I. Formulation in the frequency domain, *Journal of the Acoustical Society of America*, **103 (1)**, 49–63, (1998).

[21] Shirron, J. J. and Dey, S. Acoustic infinite elements for non-separable geometries, *Computer Methods in Applied Mechanics and Engineering*, **191**, 4123–4139, (2002).

[22] Bossut, R. and Decarpigny, J. N. Finite element modeling of radiating structures using dipolar damping element, *Journal of the Acoustical Society of America*, **86** (4), 1234–1244, (1989).

[23] Bettess, P. and Chadwick, E. Wave envelope examples for progressive waves, *International Journal for Numerical Methods in Engineering*, **38** (15), 2487–2508, (1995).

[24] Cremers, L. and Fyfe, K. R. On the use of variable order infinite wave envelope elements for acoustic radiation and scattering, *Journal of the Acoustical Society of America*, **97 (4)**, 2028–2040, (1995).

[25] Everstine, G. C. Finite element formulations of structural acoustic problems, *Computers and Structures*, **65** (3), 307–321, (1997).

[26] Gupta, A. WSMP: Watson Sparse Matrix Package Part II–direct solution of general sparse systems, *IBM Research Report RC 21888 (98472)*, (2000).

[27] Gupta, A. Recent advances in direct methods for solving unsymmetric sparse systems of linear equations, *ACM Transactions on Mathematical Software*, **28** (3), 301–324, (2002).

[28] Kinsler, L. E., Fray, A. R., Coppens, A. B., and Sanders, J. V. *Fundamentals of acoustics*, John Wiley and Sons, New York, (2000).

[29] Malecki, I. *Physical foundations of technical acoustics*, Permagon Press, Warszawa, (1969).

[30] Seybert, A. F., Wu, T. W., and Wu, X. F. Radiation and scattering of acoustic waves from elastic solids and shells using the boundary element method, *Journal of the Acoustical Society of America*, **84** (5), 1906–1912, (1988).

[31] Junger, M. C. and Feit, D. *Sound, structure, and their interactions*, MIT Press, Cambridge, (1972).

[32] Jog, C. S. Improved hybrid elements for structural analysis, *Journal of the Mechanics and Materials of Structures*, **5** (3), 507–528, (2010).

[33] Li, S. and Huang, Q. An improved form of the hypersingular boundary integral equation for exterior acoustic problems, *Engineering Analysis and Boundary Elements*, **34**, 189–195, (2010).

[34] Chen, S. H. and Liu, Y. J. A unified boundary element method for the analysis of sound and shell-like structure interactions. I. Formulation and verification, *Journal of the Acoustical Society of America*, **106** (3), 1247–1254, (1999).

[35] Skudrzyk, E. *The foundations of acoustics*, Springer-Verlag, New York, (1971).